

Article

Heat and Mass Transfer Gravity Driven Fluid Flow over a Symmetrically-Vertical Plane through Neural Networks

Fuad A. Awwad ^{1,*} , Emad A. A. Ismail ¹  and Taza Gul ^{2,3,*}

¹ Department of Quantitative Analysis, College of Business Administration, King Saud University, P.O. Box 71115, Riyadh 11587, Saudi Arabia; emadali@ksu.edu.sa

² Cambridge Graphene Center, University of Cambridge, 9 JJ Thomson Ave., Cambridge CB3 0FA, UK

³ Department of Mathematics, City University of Science and Information Technology, Peshawar 25000, Pakistan

* Correspondence: fawwad@ksu.edu.sa (F.A.A.); tazagul@cusit.edu.pk (T.G.)

Abstract: This paper explores the numerical optimization of heat and mass transfer in the buoyancy-driven Al_2O_3 -water nanofluid flow containing electrified Al_2O_3 -nanoparticles adjacent to a symmetrically-vertical plane wall. The proposed model becomes a set of nonlinear problems through similarity transformations. The nonlinear problem is solved using the *bvp4c* method. The results of the proposed model concerning heat and mass transfer with nanoparticle electrification and buoyancy parameters are depicted in the Figures and Tables. It was revealed that the electrification of nanoparticles enhances the heat and mass transfer capabilities of the Al_2O_3 water nanofluid. As a result, the electrification of nanoparticles could be an important mechanism to improve the transmission of heat and mass in the flow of Al_2O_3 -water nanofluids. Furthermore, the numerical solutions of the nanofluid model of heat/mass transfer using the deep neural network (DNN) along with the procedure of Bayesian regularization scheme (BRS), DNN-BRS, was carried out. The DNN process is provided by taking eight and ten neurons in the first and second hidden layers along with the log-sigmoid function.

Keywords: nanofluid; heat and mass transfer; electrified nanoparticles; symmetrically-vertical heated surface; neural network and BVP4



Citation: Awwad, F.A.; Ismail, E.A.A.; Gul, T. Heat and Mass Transfer Gravity Driven Fluid Flow over a Symmetrically-Vertical Plane through Neural Networks. *Symmetry* **2023**, *15*, 1288. <https://doi.org/10.3390/sym15061288>

Academic Editor: Gorakh Nath

Received: 22 May 2023

Revised: 11 June 2023

Accepted: 13 June 2023

Published: 20 June 2023



Copyright: © 2023 by the authors. Licensee MDPI, Basel, Switzerland. This article is an open access article distributed under the terms and conditions of the Creative Commons Attribution (CC BY) license (<https://creativecommons.org/licenses/by/4.0/>).

1. Introduction

Conventional working fluids cannot prevent overheating due to the increased heat output in modern systems because they require higher heat transfer rates. It happens due to the low thermal performance of the traditional fluids. The thermal performance of the fluids can be improved by dispersing the solid nanoparticles in the base solvent. To resolve this issue, a new kind of fluid, known as nanofluid, is defined by stably dispersing nanoparticles in a size range of 1 to 50 nm in conventional fluids. Choi [1] has introduced the term “nanofluid” to describe a new class of fluid, which incorporates nanoscale metallic/non-metallic particles suspended in a conventional fluid, to provide an excellent thermal improvement. The authors suspended Al_2O_3 nanoparticles in water. The enhanced thermal-physical properties of nanofluids have a substantial impact on their efficiency in convection operations. Researchers are now using these types of nanoparticles in a single base fluid to achieve promising heat transfer efficiency in the scientific domain. Thermophoresis and Brownian diffusion are defined by Buongiorno [2] for the perfection of heat transfer employing the thermal conductivity concept. He introduced the correlation between the mass, momentum, and heat transport of nanofluids. It should be noted that the nanoparticle electrification due to the Brownian diffusion of nanosized particles in a region of non-conductive fluid has been ignored. A nanofluid is a colloidal suspended nanoparticle in a base fluid. The botanists Brown [3] and Einstein [4] explained the idea of the incessant (random) motion of nanoparticles moving through molecules of a base fluid

and colliding with each other by utilizing Brownian motion. Due to Brownian motion, the particles remain suspended in the base fluid, do not settle due to gravity, and are often electrically charged, Piazza, & Parola [5] and Oakley [6]. Burton [7], deBethune [8], Hunter [9], Shaw [10], Hemsley et al. [11], Gul et al. [12,13], and Mahian et al. [14] have investigated whether the colloidal particles, when immersed into a fluid, are electrically charged in nature, owing to the preferential adsorption of common ions in the base fluid onto the surface of the colloidal particles by Van der Waals forces. Accelerating these charged particles produces both an electric and a magnetic field. Loeb [15] and Soo [16] pointed out that the Brownian distribution of solid suspended particles within a non-conducting fluid region of a particulate system creates the collision of particles and particle-wall interface, thereby ensuing in fixed electrification of the solid particles. A slightly charged particle can affect the dynamics of a particulate system. Kang and Wang [17] have suggested an appliance for augmenting the thermal conductivity of nanofluids based on the cross-coupling among the thermal motion of nanoparticles and the electric field produced nearby every charged particle. Several investigations on the formation of buoyancy-driven nanofluid flow past a vertical flat plate have already been performed (Kuznetsov and Nield [18], Khan and Aziz [19], Gorla and Chamkha [20], Aziz and Khan [21], Ahmad et al. [22], Kayalvizhi et al. [23]). Several studies on the magnetohydrodynamic (MHD) buoyancy-driven nanofluid flow along a vertical plate with several physical characteristics have been examined in recent years. Bouselsa et al. [24] examined the effects of an Al_2O_3 nanofluid flow inside a heat exchanger for the improvement of heat transfer. Slimani et al. [25] considered the inspiration of an Al_2O_3 nanofluid for energy transfer, using a conical enclosure. Anwar et al. [26] scrutinized the impact of heat source/heat sink and radiation on the flux of unstable nanofluids driven by MHD buoyancy over a moving vertical porous plate. Chandel et al. [27] explored the impact of the thermal performance of the nanofluid flow beyond a vertical surface. Arulmozhi et al. [28] looked at the effects of radiation and chemical reaction on the nanofluid flow propelled by MHD on an infinite moving vertical plate. Several researchers have studied the modeling of the buoyancy of magnetohydrodynamic (MHD)-induced nanofluids beyond a vertical plate with various physical aspects [24–28]. In all those previous MHD, the base fluid was considered electrically conducting. However, as suggested by refs. [5–17], hardly any attention has been given to the nanoparticle electrification appliance in a non-conducting base fluid when modeling the nanofluid flow. Again, research is still ongoing into increasing the thermal performance of nanofluids, which is understood from the latest available literature by Mishra et al. [29]. In polymer technology, the magnetic field strength and heat/mass transfer into the flow over a symmetrically heated surface are important theoretically and practically. This includes geothermal reservoirs, thermal insulation, porous solids drying, enhanced oil recovery, thermal insulation, nuclear reactor cooling, subwoofer catalytic reactors, enhanced oil recovery, and the rest of it. These all benefit from the joint convection device and heat flow on the vertical symmetric surface.

Fluid flow over vertical geometries has significant applications in the field of engineering. The drop in the liquid oil film is used in heavy equipment to reduce the friction force and improve the life of the machine. The electric turbine also accelerates to generate electricity due to the fluid drop. Recent problems have important implications for polymer industries, plastic film production, fiberglass production, fiber spinning, polymer sheet extraction, heat exchangers and oil production, and catalysts. The magnetic field and thermal radiation impact on the fluid flow over a liquid falling beyond a vertical symmetrically heating plate has been investigated by Ullah et al. [30], and Abbas et al. [31].

The novelty of this study was to include the concept of nanoparticle electrification in Buongiorno's model and to explore the effects of electrified Al -nanoparticles on the optimization of heat and mass transfer in buoyancy-driven Al_2O_3 -water nanofluid flow past a vertical wall, which are limited in the existing literature. It is expected that the nanoparticle electrification mechanism would not only be a new strategy for heat transport enhancement in nanofluids but would also be of great importance in designing numerous

industrial applications for nanofluids. This would be useful to determine the quality of finished products with desired properties, which highly rely on the heat transfer rate or cooling rate between the solid surface and the fluid.

Current work also aims to provide solutions for the proposed model using the deep neural network (DNN) learning process as well as the Bayesian regulation system (BRS). The DNN method was adopted with the use of ten and twenty neurons in the first and second hidden layers. The digital data set is provided with test performance, training, and verification using percentages analysis. Over the past few years, stochastic computational procedures based on neural networks have been explored using a variety of demands. Some of them represent the thermal explosion theory, including neuron analysis presented in [32] and neural networks used in fluid flow models [33,34].

- A DNN learning process was used to solve the model problem.
- The DNN training procedure is presented by taking ten and twenty neurons in the first and second hidden layers as well as the log-sigmoid activation function.
- The correctness of the procedure was observed by using the comparison between the obtained and reference results, while the negligible absolute error (AE) performances for solving the fluid model were used to enhance the worth of the scheme.

2. Materials and Methods

A steady laminar flow of buoyancy-driven Al_2O_3 -water nanofluid containing electrified alumina nanoparticles past a vertical plane wall was studied. The surface wall was taken vertically along the x -axis. T_w and C_w present the temperature and concentration of the nanofluids at the wall surface. Where C_∞ and T_∞ are the free stream components of C and T . $T_w - T_\infty > 0$ and $C_w - C_\infty > 0$ imply that the temperature and wall concentrations exceed the temperature and ambient concentration. The physical scheme is depicted in Figure 1. According to the above norms, the governing equations of the flow field in a two-dimensional cartesian coordinate system are derived from Equation (4) to Equation (8) and after boundary layer simplification following Ullah et al. [30], and Abbas et al. [31], and Pati et al. [35], are respectively expressed as.

$$\frac{\partial u}{\partial x} + \frac{\partial v}{\partial y} = 0, \quad (1)$$

$$\rho_{nf} \left[u \frac{\partial u}{\partial x} + v \frac{\partial u}{\partial y} \right] = \left(\frac{q}{m} \right) (C - C_\infty) E_x + \mu_{nf} \frac{\partial^2 u}{\partial y^2} + \beta_{f\infty} \rho_{f\infty} (T - T_\infty) (1 - C_\infty) g - (C - C_\infty) (\rho_s - \rho_{f\infty}) g, \quad (2)$$

$$\left[u \frac{\partial T}{\partial x} + v \frac{\partial T}{\partial y} \right] = \frac{k_{nf}}{(\rho c)_{nf}} \frac{\partial^2 T}{\partial y^2} + \frac{c_s D_B}{(\rho c)_{nf}} \frac{\partial C \partial T}{\partial y \partial y} + \frac{\rho_s c_s}{(\rho c)_{nf}} \frac{D_T}{T_\infty} \frac{\partial T}{\partial y} \frac{\partial T}{\partial y} + \left(\frac{q}{m} \right) \frac{c_s c}{F(\rho c)_{nf}} \left(E_x \frac{\partial T}{\partial x} + E_y \frac{\partial T}{\partial y} \right), \quad (3)$$

$$u \frac{\partial C}{\partial x} + v \frac{\partial C}{\partial y} = D_B \frac{\partial^2 C}{\partial y^2} + \frac{\rho_s D_T}{T_\infty} \frac{\partial^2 T}{\partial y^2} + \left(\frac{q}{m} \right) \frac{1}{F} \left[\frac{\partial (CE_x)}{\partial x} + \frac{\partial (CE_y)}{\partial y} \right], \quad (4)$$

$$\frac{\partial E_y}{\partial y} = \frac{q \rho_s}{m \epsilon_0}, \quad (5)$$

with suitable boundary conditions:

$$\begin{aligned} u(0) = v(0) = 0, \quad T(0) - T_w = 0, \quad C(0) - C_w = 0, \\ u(\infty) \rightarrow 0, \quad v(\infty) \rightarrow 0, \quad T(\infty) \rightarrow T_\infty, \quad C(\infty) \rightarrow C_\infty. \end{aligned} \quad (6)$$

Here u and v are the velocity components, g stands for the gravitational acceleration, β is the thermal expansion, μ is the dynamic viscosity, ρ is the density, D_B is the Brownian diffusion coefficient, D_T is the thermophoretic diffusion coefficient, (E_x, E_y) are the electric intensity components, (ρc) is the specific heat. $u(0)$, $v(0)$, $T(0)$, $C(0)$ are the initial velocity, temperature, and concentration conditions. $u(\infty)$, $v(\infty)$, $T(\infty)$, $C(\infty)$ are the boundary conditions for velocity, temperature, and concentration.

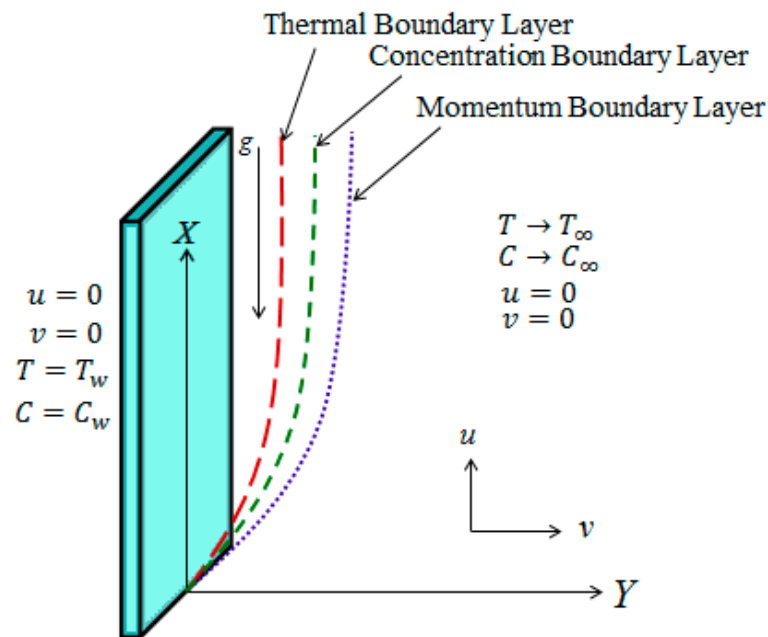


Figure 1. The geometry of the problem.

The Equations (1)–(6) are transformed using the concept of stream function as suggested by Soo [16]. Equation (1) is satisfied by the introduction of the stream function $\psi(x, y) = \alpha_f (Ra_x)^{\frac{1}{4}} f(\eta)$. Whereas, the velocity components $u = \frac{\partial \psi}{\partial y}$, and $v = -\frac{\partial \psi}{\partial x}$ are selected from the stream function for the transformation of the rest of the Equations (2)–(6). Moreover, $Ra_x = \frac{B_f g (T_w - T_\infty) (1 - C_\infty) x^3}{\nu_f \alpha_f}$ denotes the local Rayleigh number. These similarity variables are also used by Kuznetsov and Nield [18] for the transformations and are defined as:

$$\eta = \frac{y}{x} (Ra_x)^{\frac{1}{4}}, \quad u = \frac{(Ra_x)^{0.5} \alpha_f}{x} f', \quad v = -\frac{(Ra_x)^{0.5} \alpha_f}{x} [\eta f' - 3f], \quad (7)$$

$$S(\eta)(C_w - C_\infty) = C - C_\infty, \quad \theta(\eta)(T_w - T_\infty) = T - T_\infty.$$

The non-dimensional Equations (2)–(4) and the boundary Equation (5) are expressed as the following equations:

$$f''' + \frac{1}{\varphi_s} (\theta - NrS) + \varphi_1 \varphi_2 \frac{M Sc Nb}{pr N_F} S + \frac{\varphi_1}{4Pr} [3ff''' - 2(f')^2] = 0, \quad (8)$$

$$\theta'' + \frac{1}{\varphi_4} Sc Nb \left[\frac{N_F}{N_{Re}} - \frac{1}{4} M \right] (S + Nc) \eta \theta' + \frac{3}{4} \frac{1}{\varphi_3 \varphi_4} f \theta' + \frac{1}{\varphi_4} Pr Nt (\theta')^2 + \frac{1}{\varphi_4} Pr Nb S' \theta' = 0, \quad (9)$$

$$S'' + \frac{N_F Sc}{Pr N_{Re}} (\eta S' + S + Nc) - \frac{1}{4} \frac{M Sc}{Pr} \eta S' + \frac{Nt}{Nb} \theta'' + \frac{3}{4} \frac{Sc}{Pr} f S' = 0, \quad (10)$$

with the boundary conditions:

$$\begin{aligned} \eta = 0 : f = f' = 0, \quad \theta = 1, \quad S = 1, \\ \eta \rightarrow \infty : f' \rightarrow 0, \quad \theta \rightarrow 0, \quad S \rightarrow 0. \end{aligned} \quad (11)$$

The preceding equations are the form of transformation of the suggested model. The embedded parameters appearing in Equations (8)–(10) are demonstrated below and mentioned in (Maharukh et al., [36]):

$$\begin{aligned} \text{Pr} &= \frac{\nu_f}{\alpha_f}, \quad \text{Sc} = \frac{\nu_f}{D_B}, \quad \text{Nr} = \frac{(\rho_s - \rho_f)(C_w - C_\infty)}{(1 - C_\infty)\rho_f\beta_f(T_w - T_\infty)}, \quad \text{Nb} = \frac{(\rho c)_s(C_w - C_\infty)D_B}{(\rho c)_f\nu_f}, \\ \frac{1}{\text{NRe}} &= \left(\frac{q}{m}\right)^2 \frac{\rho_s}{\varepsilon_0} x^2 \left(\frac{x}{\alpha_f(Ra_x)^{\frac{1}{2}}}\right)^2, \quad \text{Nf} = \text{F}x \left(\frac{\alpha_f(Ra_x)^{\frac{1}{2}}}{x}\right), \quad \text{Nc} = \frac{C_\infty}{(C_w - C_\infty)}, \\ M &= \frac{1}{F} \left(\frac{q}{m}\right) \left(\frac{x}{\alpha_f(Ra_x)^{\frac{1}{2}}}\right) E_x, \quad \text{Nt} = \frac{(\rho c)_s(T_w - T_\infty)D_T}{(\rho c)_f\nu_f T_\infty}, \end{aligned} \quad (12)$$

here Pr , Sc , Nr , Nb , NRe , Nf , Nc , M , Nt , are the Prandtl number, Schmidt number, buoyancy ratio, Brownian motion parameter, momentum transfer number, concentration ratio, nanoparticle ionization parameter, and thermophoresis parameter, respectively.

The thermophysical properties are defined as:

$$\begin{aligned} \varphi_1 &= \frac{\mu_f}{\mu_{nf}} \frac{\rho_{nf}}{\rho_f} = (1 - c_\infty)^{2.5} \left[c_\infty \frac{\rho_s}{\rho_f} + (1 - c_\infty) \right], \quad \varphi_2 = \frac{c_f}{c_s} \left[c_\infty \frac{\rho_s}{\rho_f} + (1 - c_\infty) \right]^{-1}, \quad \tau = \frac{(\rho c)_s}{(\rho c)_f}, \\ \varphi_3 &= \frac{(\rho c)_f}{(\rho c)_{nf}} = \frac{1}{c_\infty \tau + (1 - c_\infty)}, \quad \varphi_4 = \frac{k_{nf}}{k_f} = \frac{2k_f + k_s - 2c_\infty(k_f - k_s)}{2k_f + k_s + c_\infty(k_f - k_s)}, \quad \varphi_5 = \frac{\mu_{nf}}{\mu_f} = \frac{1}{(1 - c_\infty)^{2.5}}. \end{aligned} \quad (13)$$

The nanofluid used in this investigation is water-based and contains 1% alumina nanoparticles (when compared to pure water). Table 1 shows the Al_2O_3 -water nanofluid thermophysical properties.

Table 1. The values of the thermophysical properties.

Property	Solid (Alumina)	Fluid (Water)
c_p (J/kgk)	765	4179
k (W/mk)	40	0.613
ρ (kg/m ³)	3970	997.1

For heat transfer applications, the local Nusselt number is exhibited as $Nu_x = \frac{xq_w}{k_f(T_w - T_\infty)}$, $q_m = -k_f \left(\frac{\partial T}{\partial y}\right)_{y=0}$ is the wall heat flux. For mass transfer applications, the local Sherwood number sh_x is exhibited as, $sh_x = \frac{xq_w}{D_B(C_w - C_\infty)}$, where $q_m = -D_B \left(\frac{\partial c}{\partial y}\right)_{y=0}$ is the wall mass flux. In dimensionless form, the heat transfer $-\theta'(0)$ and the mass transfer $-S'(0)$ are, respectively, expressed as:

$$-\theta'(0) = Nu_x / Ra_x^{\frac{1}{4}} \text{ and } -S'(0) = sh_x / Ra_x^{\frac{1}{4}}. \quad (14)$$

3. Results

The buoyancy-driven nanofluid flow past a vertical wall was considered for the applications of heat and mass transfer. In a steady laminar flow of buoyancy-driven fluid past a vertical plane wall with a magnetic field provided perpendicular to the fluid flow, the magnetic parameter can have significant effects on the velocity, temperature, and concentration profiles of the fluid. As the increasing magnetic parameter rises the resistance force, the fluid flow is opposed. This can induce Lorentz forces that modify the flow behavior and lead to changes in the velocity, temperature, and concentration profiles. Specifically, in this scenario, the buoyancy-driven fluid flow is characterized by natural convection induced by a temperature difference between the wall and the surrounding fluid. The magnetic field can interact with this flow and modify it in the described ways. As the magnetic field becomes stronger, it can suppress the natural convection and introduce a new flow pattern dominated by the Lorentz forces. This can cause changes in the velocity profile, which may become more uniform near the wall and more peaked near the centreline.

The temperature profile can also be affected by the magnetic field, particularly in the high magnetic Reynolds number regime as shown in Figure 2. The Lorentz forces can induce heat transfer enhancement or suppression depending on the direction of the magnetic field and relative to the temperature gradient. This can lead to changes in the temperature profile, which may become more uniform near the wall or develop a central temperature peak. The concentration profile of a fluid can also be influenced by the magnetic field, particularly when the fluid is a mixture of different components. The Lorentz forces can cause differences in the diffusion rates of the components and modify the concentration profile of the fluid. Therefore, the magnetic parameter can have significant effects on the velocity, temperature, and concentration profiles of a buoyancy-driven fluid flow past a vertical plane wall. The specific changes depend on the strength of the magnetic field and its interaction with the flow dynamics. The Brownian motion effect in terms of the Brownian parameter Nb has been displayed in Figure 3 and for Nf impact in Figure 4 versus fluid motion, thermal profile, and concentration field. The fluid motion slightly increased with the increasing values of Nb , and Nf , while the same effect was observed for the thermal profile. However, a decline in effect was observed for the concentration profile, as shown in the last part of Figures 3 and 4. Physically, the boundary layer thickness was dependent on the thermal boundary condition at the outer surface. Therefore, the fluid motion upsurges and the concentration profile declines. The Buoyancy ratio parameter effect, in terms of the Brownian parameter Nr , is displayed in Figure 5 versus nanofluid flow, thermal profile, and concentration field. Physically, the Buoyancy ratio parameter opposes the pressure gradient, and consequently, reduces the fluid motion.

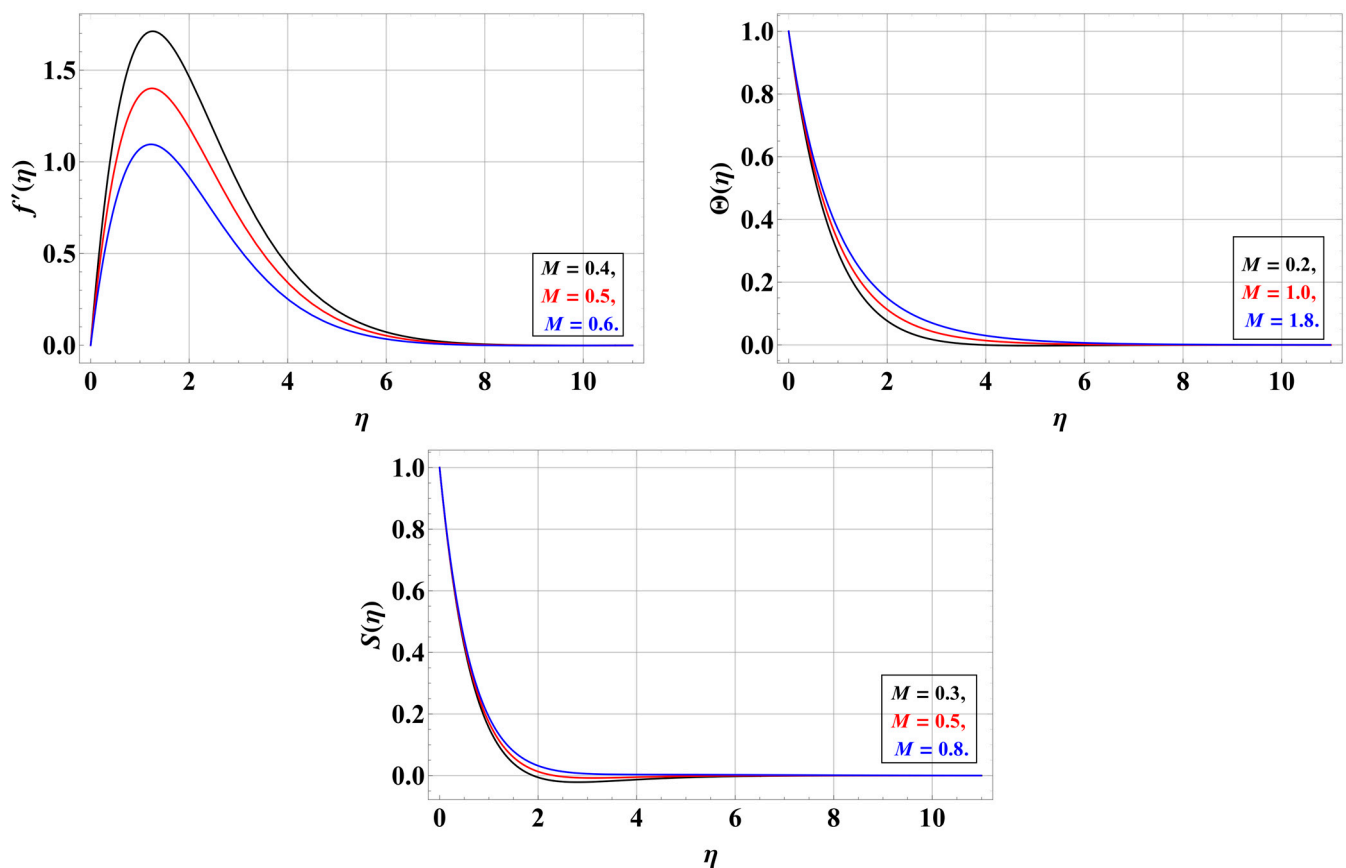


Figure 2. M VS f' , θ , S .

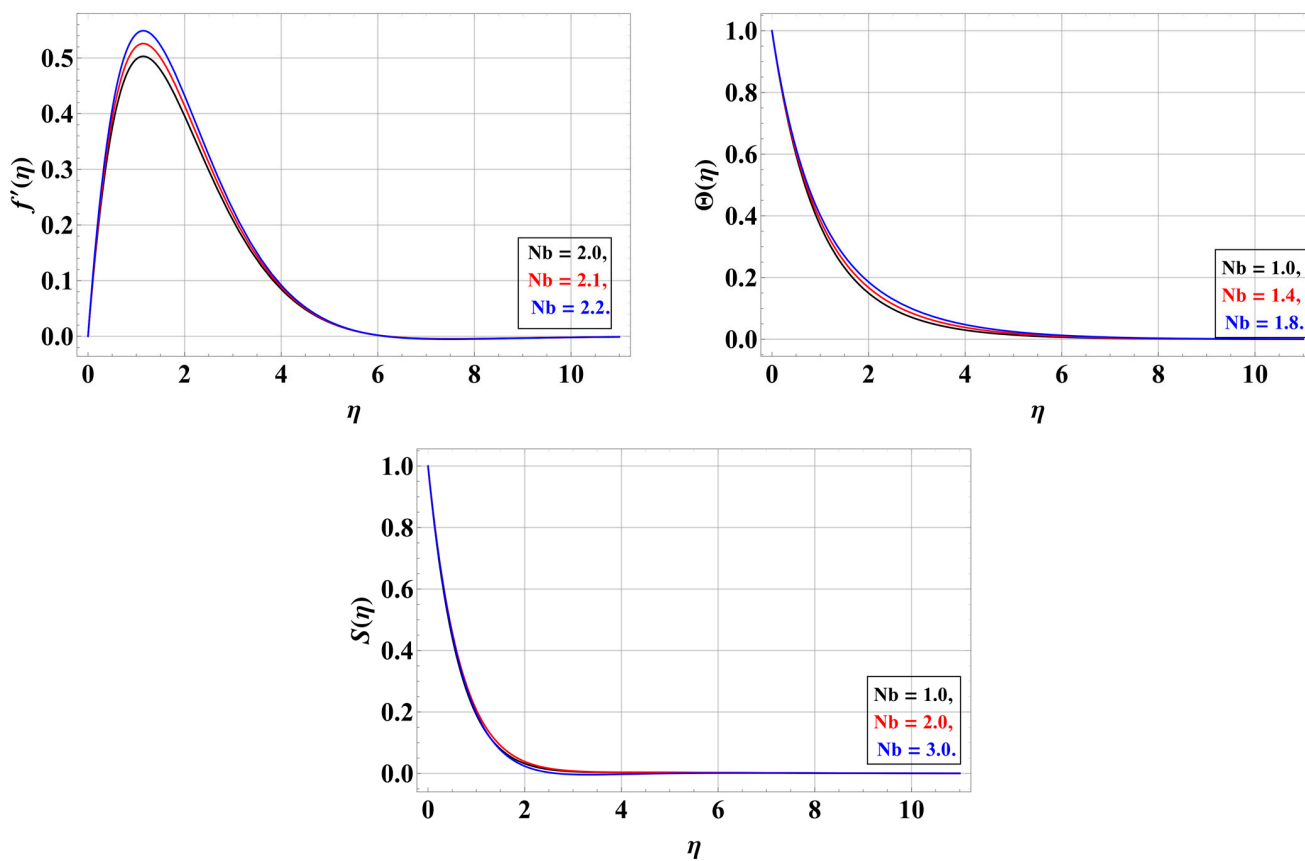


Figure 3. Nb VS f' , θ , S .

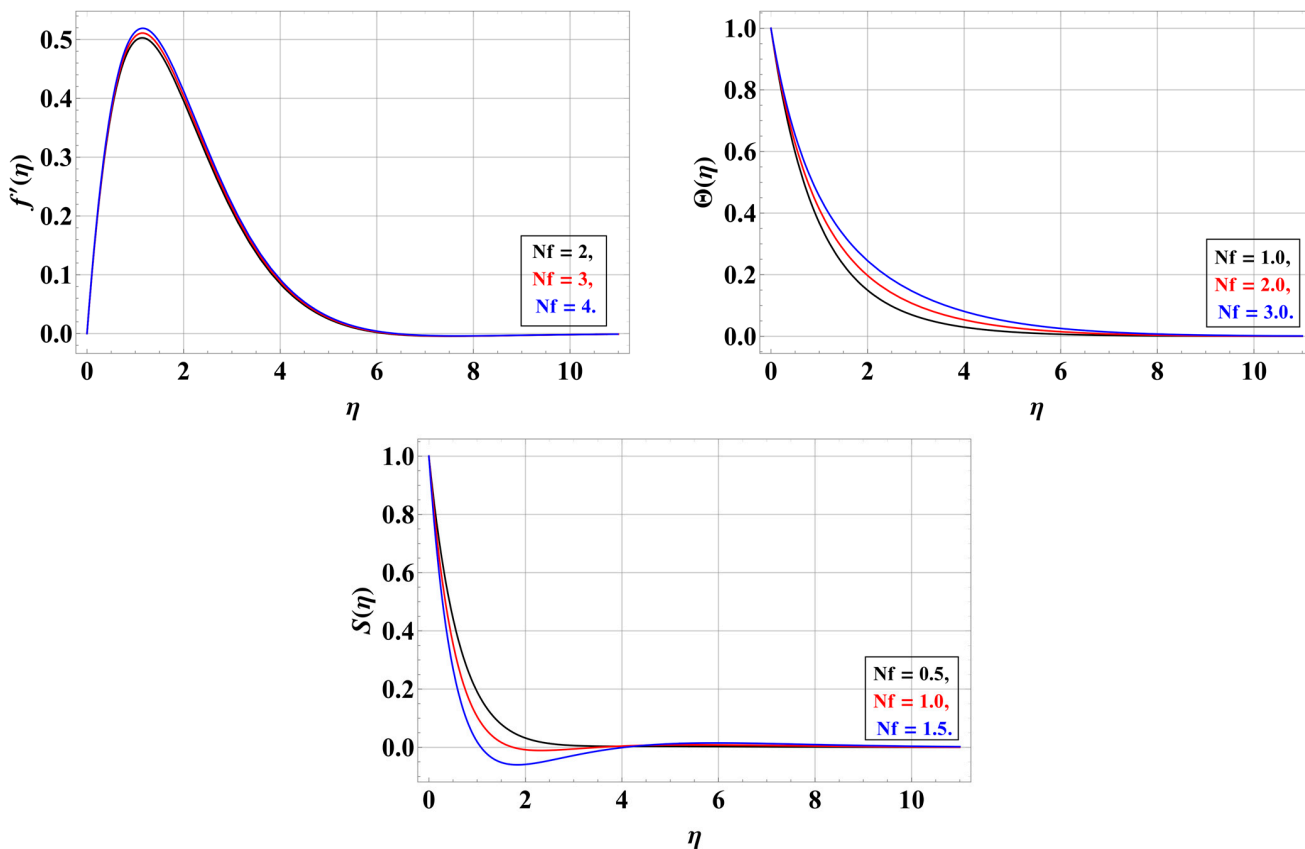


Figure 4. Nf VS f' , θ , S .

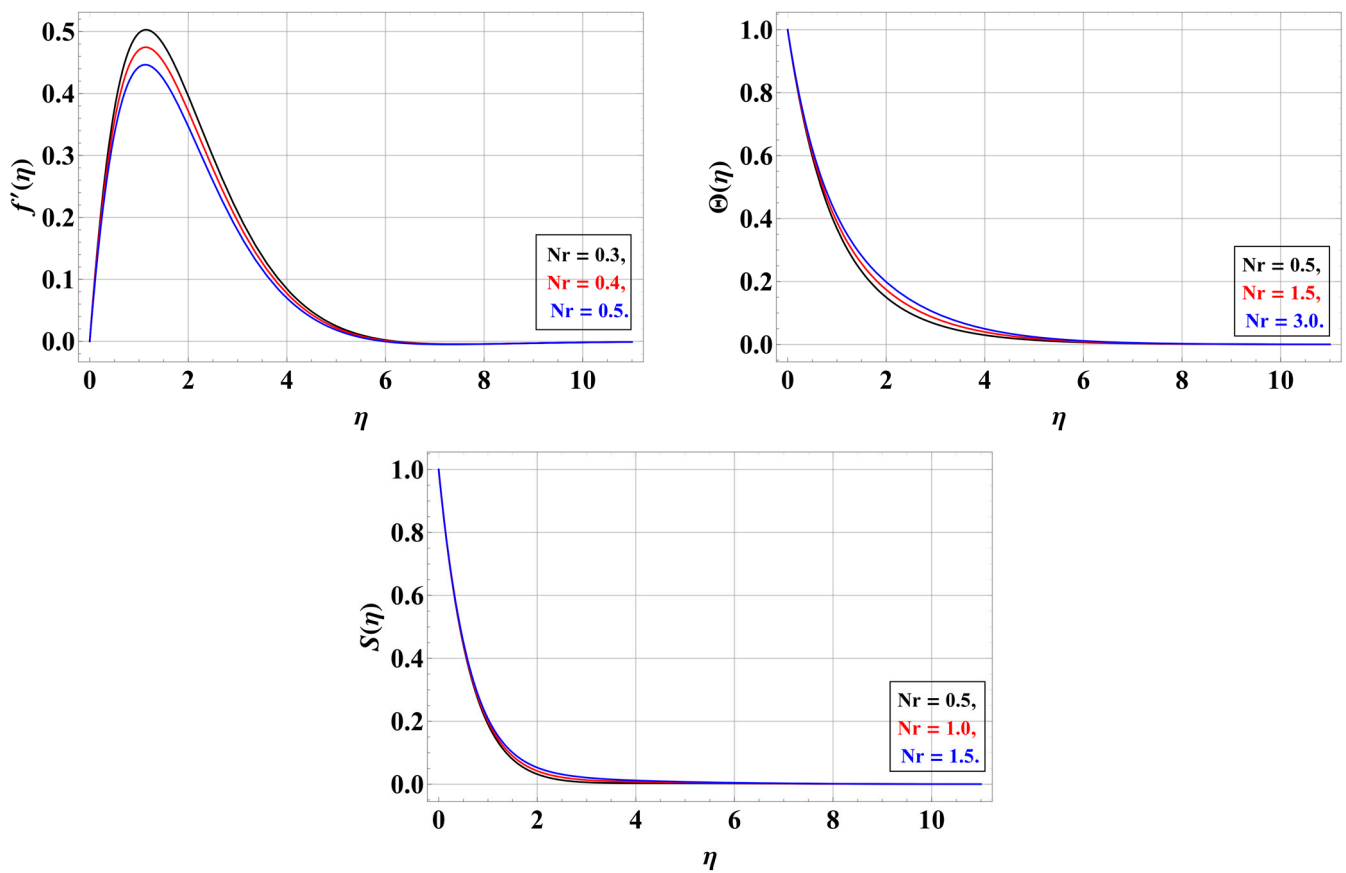


Figure 5. Nr VS f' , θ , S .

Neural Networks

The purpose of this study was to present numerical solutions for the nanofluid model of heat/mass transfer using the deep neural network (DNN) along with the procedure of Bayesian regularization scheme (BRS), DNN-BRS, as described in [37–41]. The DNN process was delivered by taking eight and ten neurons into the first and second hidden layers as well as the log-sigmoid function. The numerical data set was provided using the Adam method, which was performed through testing, training, and verification processes. The model was categorized into three categories: a dimensionless form of the stream, a concentration state, and temperature. The accuracy of the DNN-BRS solver was observed by comparing the benchmark and offering solutions. Reliability and accuracy were achieved through negligible absolute error values. The numerical observations obtained from the fluid model were calculated to reduce the efficiency of the mean square error. The competence and reliability of the DNN-BRS solver were validated by relative measures of state transitions (STs), regression, error histograms, and correlation.

In Figure 6, the DNN approach was used to handle the nonlinear problem. The input layers were 8, while the hidden layers were 10, sigmoid activation function, and 1 output layer. It is evident from the above-stated strategy that the Bayesian regularization artificial neural networks (BR-ANNs) is a more efficient and advanced technique to solve the nonlinear problems that arise in the field of science and engineering. This strategy tends to reduce lengthy calculations and minimize problem solutions through high accuracy and convergence. BRS is a mathematical procedure that transforms nonlinear regression into a single statistical problem by utilizing the peak regression process.

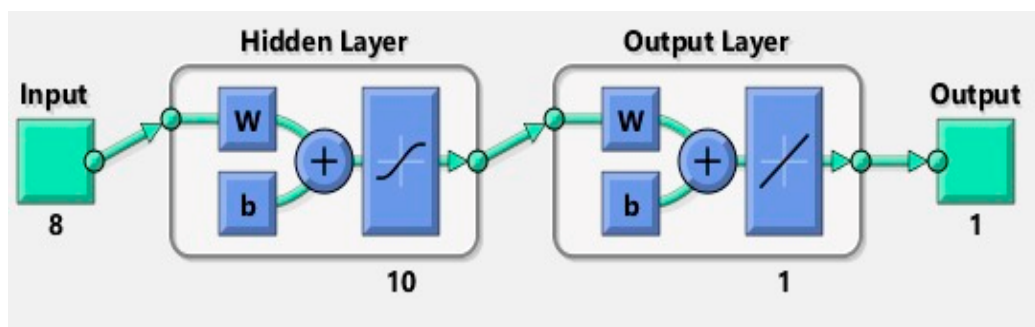


Figure 6. DNN learning approach for the heat and mass transfer problem.

Figures 7–11 apply the DNN-BRS. Figure 7 shows the MSE training performances for each case in the heat/mass transfer WNF model, which were calculated as 2.321×10^{-10} , and 1.5321×10^{-10} at epochs 678, and 903, respectively. Figure 8 represents the gradient, μ , num parameter, sum squared, and validation checks for the respective cases in the heat/mass transfer WNF system. The gradient calculated for cases 1 to 2 were 1.3556×10^{-06} , and 3.6828×10^{-07} . Figure 9 presents the function fitness for solving the fluid model using the DNNs-BRS of cases 1 to 2. The performances of the EHs for the fluid dynamics system using DNNs-BRS are plotted in Figure 10. These EHs values for the respective variations of the model were obtained at 1.84×10^{-06} , and 5.89×10^{-06} . The regression values for cases 1 to 2 are illustrated in Figures 10 and 11 for solving the fluid model using the DNNs-BRS. These values for each case are presented as one for each case of the model that represents the perfect modeling.

The calculated impact of the various parameters versus heat and mass transfer rates is shown in Table 2. Nt, Nb, Nc , increase the heat transfer rate for its larger values. The greater values of Nb decrease the mass transfer rate, while Nt & Sc increase the Sherwood number.

Table 2. Heat and mass transfer in terms of embedded parameters impact.

Parameters				$\theta'(0)$	$S'(0)$
Nt	Nc	Nb	Sc		
0.1	0.01	0.1	0.1	0.38356	0.370880
0.3				0.418340	0.3781709
0.5				0.434021	0.381703
	0.02			0.43194	0.370880
	0.03			0.478149	0.370880
		0.2		0.3973194	0.3642471
		0.3		0.408781	0.3513482
			0.2	0.38356	0.421032
			0.3	0.38356	0.4421872

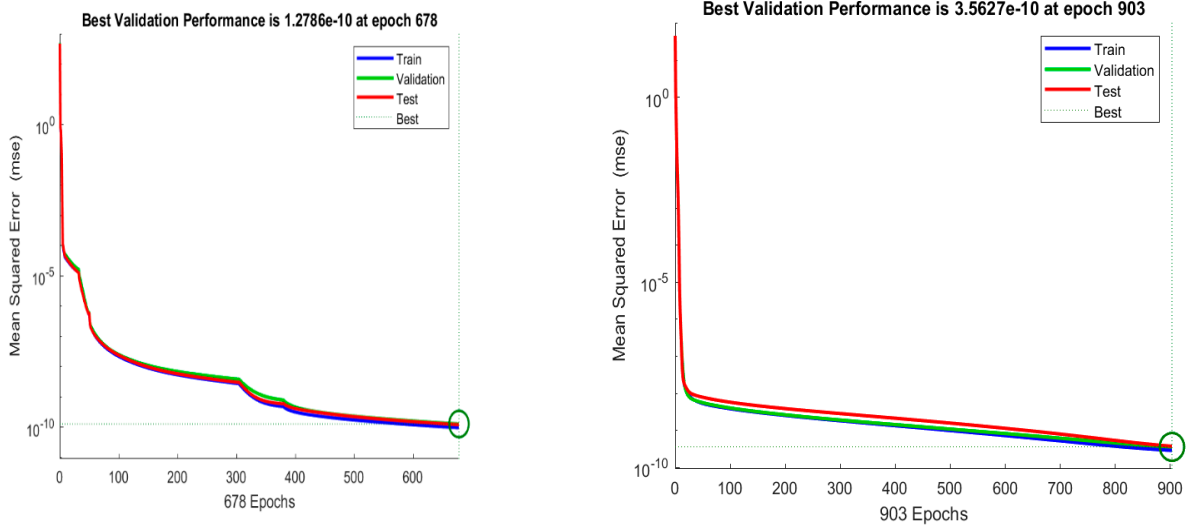


Figure 7. MSE measure for the solution of the nonlinear problem.

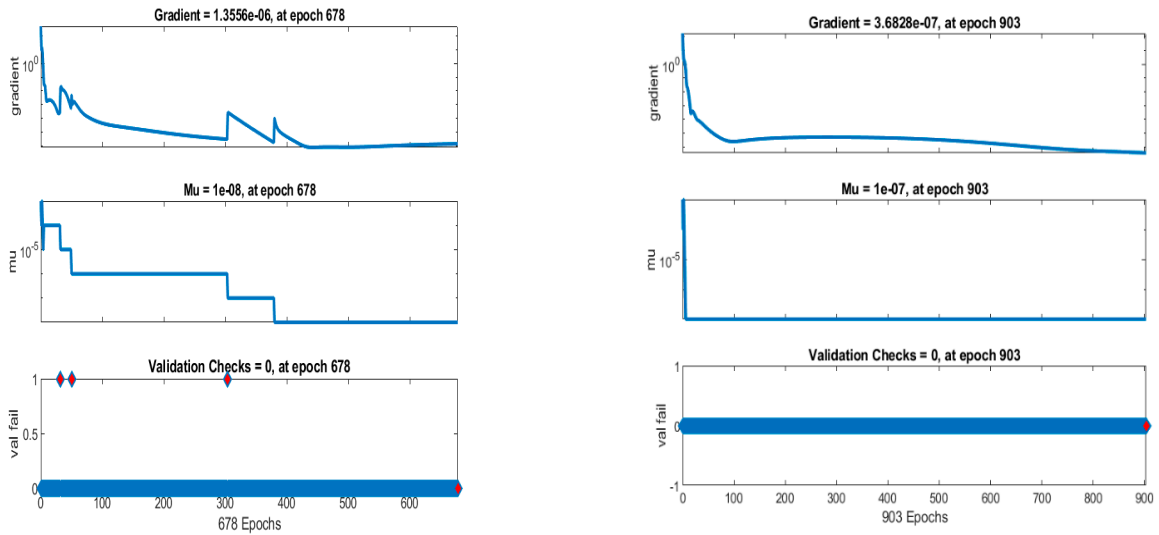


Figure 8. STs for solving the model using the DNNs-BRS.

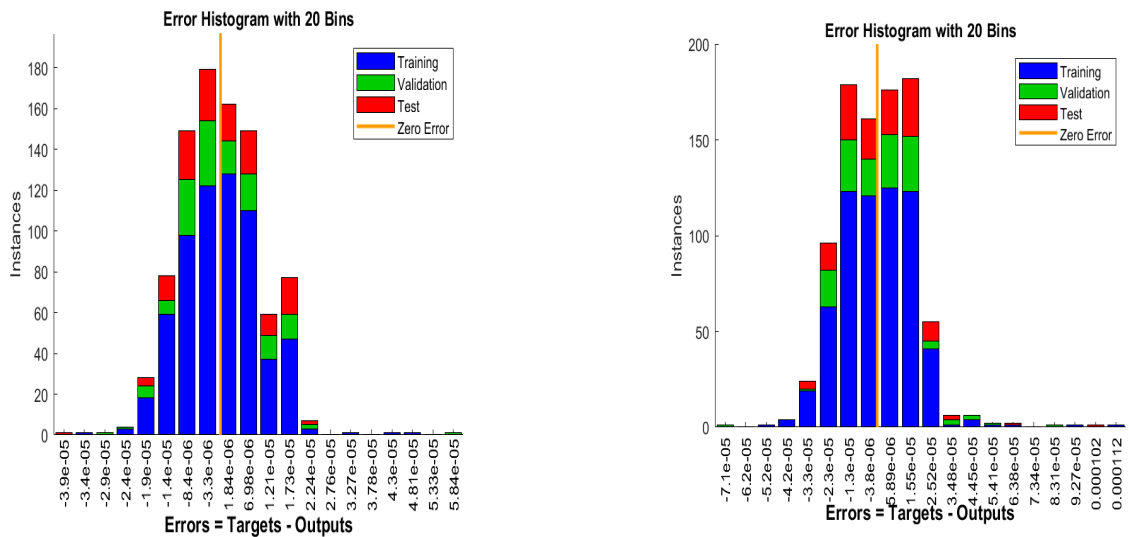


Figure 9. EHs performance.

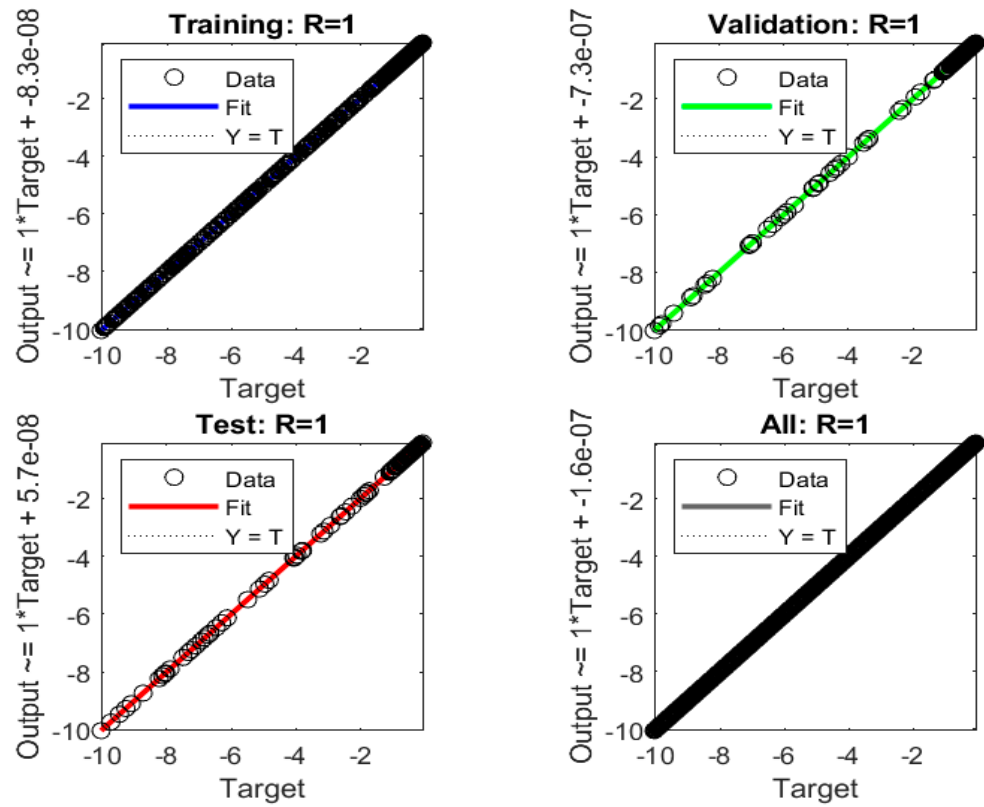


Figure 10. Regression performances in the first case.

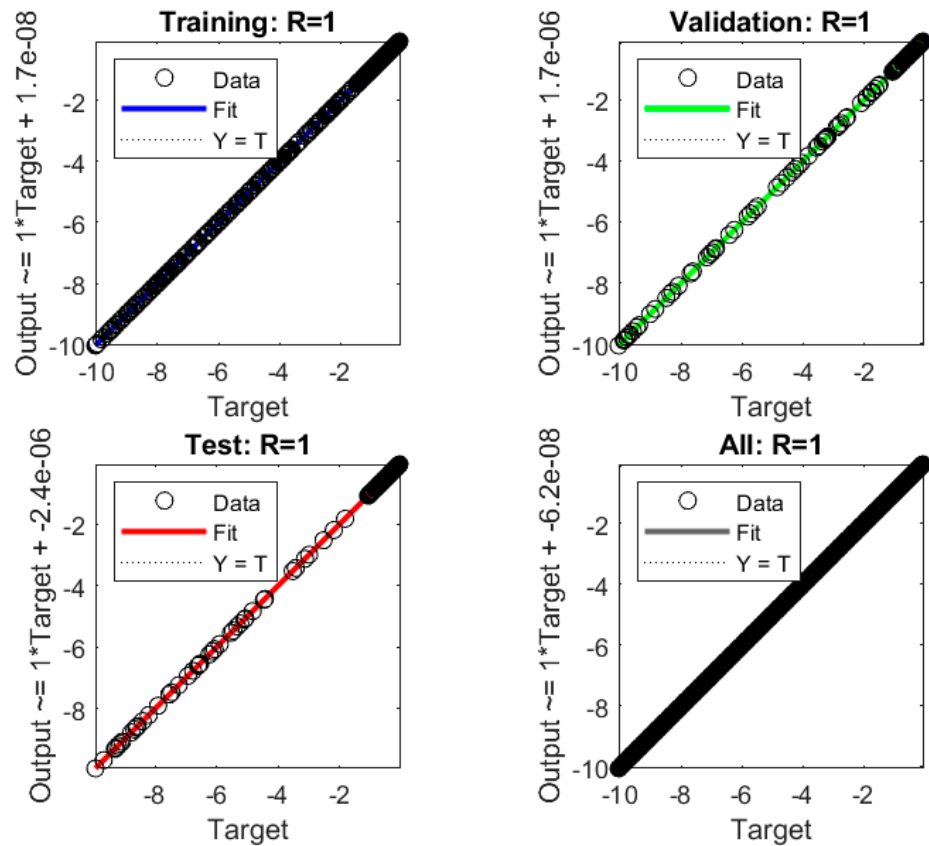


Figure 11. Regression performances in the second case.

4. Conclusions

In the numerical simulation of buoyancy-driven Al_2O_3 -water nanofluid flow containing electrified Al_2O_3 -nanoparticles adjacent to a symmetrically vertical plane wall, the impacts of Al_2O_3 nanoparticle electrification parameter M and buoyancy ratio Nr on non-dimensional concentration, temperature, and velocity profiles, as well as dimensionless coefficients of heat and mass transfer have been thoroughly examined. The concluding results show that the heat transfer rate increased with the inclusion of the Al_2O_3 nanoparticles in the base fluid of water. The significant results are highlighted herewith.

- An increase in M causes the velocity of the nanofluid in the boundary layer region to increase, whereas an increase in Nr causes the velocity to decrease.
- An increase in Nr raises the temperature of the nanofluid, whereas an increase in M lowers the temperature near the plane wall.
- In the vicinity of the plane wall, increasing Nr enhances the concentration of nanoparticles, while increasing M reduces the concentration.
- The dimensionless heat and mass transfer coefficients of the nanofluid rise alongside M , while both reduce with Nr .
- The process of DNN is presented in two hidden layers, with 8 and 10 neurons, to solve the model.
- The log-sigmoid function is used as an activation function for both hidden layers to solve the mathematical model.
- The reliability and exactness are observed through the negligible values of the absolute error for each variation of the model.
- The numerical achieved observations of the fluid dynamical system have been computed to reduce the mean square error performances, which were performed in negligible values for the testing and training.

Author Contributions: F.A.A.: Supervision, software, conceptualization, writing—original draft and writing—review and editing; E.A.A.I.: Validation, modeling, methodology, writing—original draft and writing—review and editing; T.G.: Writing—original draft and writing—review and editing. All authors have read and agreed to the published version of the manuscript.

Funding: This project (RSPD2023R576) is funded by King Saud University, Riyadh, Saudi Arabia.

Data Availability Statement: The datasets used and/or analyzed during the current study are available from the corresponding author on reasonable request.

Acknowledgments: Researchers Supporting Project number (RSPD2023R576), King Saud University, Riyadh, Saudi Arabia.

Conflicts of Interest: The authors declare no conflict of interest.

Nomenclature

List of symbols

u, v —Components of velocity (ms^{-1}).
 Sc —Schmidt number
 D_B —Brownian diffusion coefficient (m^2/s).
 (E_x, E_y) —Electric intensity (N/C).
 Nr —Buoyancy ratio.
 T —Temperature of fluid (K).
 Pr —Prandtl number.
 D_T —Thermophoretic coefficient (m^2s^{-1}).
 Nb —Brownian motion parameter.
 g —Gravitational acceleration (ms^{-2}).
 Nc —Nanoparticle ionization parameter
 T_w, T_∞ —Lower, Upper wall temperature (K).
 N_{Re} —Momentum transfer number.

Greek symbols

μ_{nf} —The viscosity of nanofluid (mPa).
 ϕ —Nanoparticle volume fraction
 η —Dimensionless transform variable
 cp_f —Heat capacitance (J/kg · K).
 k_{nf} —Thermal conductivity (W/mK).
 α —Stretching shrinking parameter
 cp_{nf} —Heat capacitance of nanofluid
 ρ_f —Base fluid density (Kgm^{-3}).
 μ_f —Viscosity of the base fluid (mPa).
 σ_{nf} —Electrical conductivity
 ρ_{nf} —Hybrid nanofluid density (Kgm^{-3}).
 β_T —Thermal expansion (K^{-1}).
 Θ, f —Dimensional thermal, velocity fields

References

1. Choi, U.S. *Enhancing Thermal Conductivity of Fluids with Nanoparticles*; AS-MEFED; Argonne National Lab. (ANL): Argonne, IL, USA, 1995; Volume 231, pp. 99–105.
2. Boungiorno, J. Convective transport in nanofluids. *ASME J. Heat Transfer* **2006**, *128*, 240–250. [[CrossRef](#)]
3. Brown, R. XXVII. A brief account of microscopical observations made in the months of June, July and August 1827, on the particles contained in the pollen of plants; and on the general existence of active molecules in organic and inorganic bodies. *Philos. Mag.* **1828**, *4*, 161–173. [[CrossRef](#)]
4. Einstein, A. *Investigations on the Theory of the Brownian Movement*; Courier Corporation: Chelmsford, MA, USA, 1956.
5. Piazza, R.; Parola, A. Thermophoresis in colloidal suspensions. *J. Phys. Condens. Matter* **2008**, *20*, 153102. [[CrossRef](#)]
6. Oakley, H.B. The Origin of the Charge on Colloidal Particles. *J. Phys. Chem.* **1926**, *30*, 902–916. [[CrossRef](#)]
7. Burton, E.F. *The Physical Properties of Colloidal Solutions*; Longmans Green: London, UK, 1921.
8. deBethune, A.J.; Licht, T.S.; Swendeman, N. The temperature coefficients of electrode potentials. *J. Electrochem. Soc.* **1959**, *106*, 616. [[CrossRef](#)]
9. Hunter, R.J. *Zeta Potential in Colloid Science: Principles and Applications*; Academic Press: Cambridge, MA, USA, 2013.
10. Shaw, D.J. *Introduction to Colloid and Surface Chemistry*; Butterworths: Oxford, UK, 1980.
11. Hemsley, A.R.; Collinson, M.E.; Kovach, W.L.; Vincent, B.; Williams, T. The role of self-assembly in biological systems: Evidence from iridescent colloidal sporopollenin in Selaginella megaspore walls. *Philos. Trans. R. Soc. Lond. B Biol. Sci.* **1994**, *345*, 163–173.
12. Gul, T.; Khan, M.A.; Noman, W.; Khan, I.; Abdullah Alkanhal, T.; Tlili, I. Fractional order forced convection carbon nanotube nanofluid flow passing over a thin needle. *Symmetry* **2019**, *11*, 312. [[CrossRef](#)]
13. Gul, T.; Anwar, H.; Khan, M.A.; Khan, I.; Kumam, P. Integer and non-integer order study of the GO-W/GO-EG nanofluids flow by means of Marangoni convection. *Symmetry* **2019**, *11*, 640. [[CrossRef](#)]
14. Mahian, O.; Kolsi, L.; Amani, M.; Estellé, P.; Ahmadi, G.; Kleinstreuer, C.; Marshall, J.S.; Siavashi, M.; Taylor, R.A.; Niazmand, H.; et al. Recent advances in modeling and simulation of nanofluid flows-Part I: Fundamentals and theory. *Phys. Rep.* **2019**, *790*, 1–48. [[CrossRef](#)]
15. Loeb, L.B. The generation of static charges by processes involving ionization of gases. In *Static Electrification*; Springer: Berlin/Heidelberg, Germany, 1958; pp. 201–224.
16. Soo, S.L. Effect of electrification on the dynamics of a particulate system. *Ind. Eng. Chem. Fundam.* **1964**, *3*, 64–68. [[CrossRef](#)]
17. Kang, Z.; Wang, L. Effect of thermal-electric cross coupling on heat transport in nanofluids. *Energies* **2017**, *10*, 123. [[CrossRef](#)]
18. Kuznetsov, A.V.; Nield, D.A. Natural convective boundary-layer flow of a nanofluid past a vertical plate. *Int. J. Therm. Sci.* **2010**, *49*, 243–247. [[CrossRef](#)]
19. Khan, W.A.; Aziz, A. Natural convection flow of a nanofluid over a vertical plate with uniform surface heat flux. *Int. J. Therm. Sci.* **2011**, *50*, 1207–1214. [[CrossRef](#)]
20. Gorla, R.S.R.; Chamkha, A. Natural convective boundary layer flow over a nonisothermal vertical plate embedded in a porous medium saturated with a nanofluid. *Nanoscale Microscale Thermophys. Eng.* **2011**, *15*, 81–94. [[CrossRef](#)]
21. Aziz, A.; Khan, W.A. Natural convective boundary layer flow of a nanofluid past a convectively heated vertical plate. *Int. J. Therm. Sci.* **2012**, *52*, 83–90. [[CrossRef](#)]
22. Ahmad, R.; Mustafa, M.; Turkyilmazoglu, M. Buoyancy effects on nanofluid flow past a convectively heated vertical Riga-plate: A numerical study. *Int. J. Heat Mass Transf.* **2017**, *111*, 827–835. [[CrossRef](#)]
23. Kayalvizhi, J.; Vijaya Kumar, A.G.; Öztop, H.F.; Sene, N.; Abu-Hamdeh, N.H. Heat Transfer Enhancement through Thermodynamical Activity of H₂O/Clay Nanofluid Flow over an Infinite Upright Plate with Caputo Fractional-Order Derivative. *Energies* **2022**, *15*, 6082. [[CrossRef](#)]
24. Bouselsal, M.; Mebarek-Oudina, F.; Biswas, N.; Ismail, A.A.I. Heat Transfer Enhancement Using Al₂O₃-MWCNT Hybrid-Nanofluid inside a Tube/Shell Heat Exchanger with Different Tube Shapes. *Micromachines* **2023**, *14*, 1072. [[CrossRef](#)]
25. Slimani, R.; Aissa, A.; Mebarek-Oudina, F.; Khan, U.; Sahnoun, M.; Chamkha, A.J.; Medebber, M.A. Natural convection analysis flow of Al₂O₃-Cu/water hybrid nanofluid in a porous conical enclosure subjected to the magnetic field. *Eur. Phys. J. Appl. Phys.* **2020**, *92*, 10904. [[CrossRef](#)]
26. Anwar, T.; Kumam, P.; Shah, Z.; Watthayu, W.; Thounthong, P. Unsteady radiative natural convective MHD nanofluid flow past a porous moving vertical plate with heat source/sink. *Molecules* **2020**, *25*, 854. [[CrossRef](#)]
27. Chandel, S.; Sood, S. Numerical analysis of Williamson-micropolar nanofluid flow through porous rotatory surface with slip boundary conditions. *Int. J. Appl. Comput. Math.* **2022**, *8*, 134. [[CrossRef](#)]
28. Arulmozhi, S.; Sukkiramathi, K.; Santra, S.S.; Edwan, R.; Fernandez-Gamiz, U.; Noeiaghdam, S. Heat and mass transfer analysis of radiative and chemical reactive effects on MHD nanofluid over an infinite moving vertical plate. *Results Eng.* **2022**, *14*, 100394. [[CrossRef](#)]
29. Mishra, S.; Nayak, M.; Misra, A. Thermal conductivity of nanofluids—A comprehensive review. *Int. J. Thermofluid Sci. Technol.* **2020**, *7*, 070301. [[CrossRef](#)]
30. Ullah, Z.; Bilal, M.; Sarris, I.E.; Hussanan, A. MHD and Thermal Slip Effects on Viscous Fluid over Symmetrically Vertical Heated Plate in Porous Medium: Keller Box Analysis. *Symmetry* **2022**, *14*, 2421. [[CrossRef](#)]

31. Abbas, A.; Ashraf, M.; Sarris, I.E.; Ghachem, K.; Labidi, T.; Kolsi, L.; Ahmad, H. Numerical Simulation of the Effects of Reduced Gravity, Radiation and Magnetic Field on Heat Transfer Past a Solid Sphere Using Finite Difference Method. *Symmetry* **2023**, *15*, 772. [[CrossRef](#)]
32. Sabir, Z. Neuron analysis through the swarming procedures for the singular two-point boundary value problems arising in the theory of thermal explosion. *Eur. Phys. J. Plus* **2022**, *137*, 638. [[CrossRef](#)]
33. Shoaib, M.; Naz, S.; Nisar, K.S.; Raja, M.A.Z.; Aslam, S.; Ahmad, I. MHD Casson Nanofluid in Darcy-Forchheimer Porous Medium in the Presence of Heat Source and Arrhenious Activation Energy: Applications of Neural Networks. *Int. J. Model. Simul.* **2022**, *43*, 1–24. [[CrossRef](#)]
34. Raja, M.A.Z.; Shoaib, M.; Khan, Z.; Zuhra, S.; Saleel, C.A.; Nisar, K.S. Supervised neural networks learning algorithm for three dimensional hybrid nanofluid flow with radiative heat and mass fluxes. *Ain Shams Eng. J.* **2022**, *13*, 101573. [[CrossRef](#)]
35. Ramanuja, M.; Kavitha, J.; Sudhakar, A.; Radhika, N. Study of MHD SWCNT-Blood Nanofluid Flow in Presence of Viscous Dissipation and Radiation Effects through Porous Medium. *J. Niger. Soc. Phys. Sci.* **2023**, *5*, 1054. [[CrossRef](#)]
36. Mahrukh, M.; Kumar, A.; Gu, S.; Kamnis, S.; Gozali, E. Modeling the effects of concentration of solid nanoparticles in liquid feedstock injection on high-velocity suspension flame spray process. *Ind. Eng. Chem. Res.* **2016**, *55*, 2556–2573. [[CrossRef](#)]
37. Shoaib, M.; Kainat, R.; Ijaz Khan, M.; Prasanna Kumara, B.C.; Naveen Kumar, R.; Zahoor Raja, M.A. Darcy-Forchheimer entropy-based hybrid nanofluid flow over a stretchable surface: Intelligent computing approach. *Waves Random Complex Media* **2022**, 1–24. [[CrossRef](#)]
38. Raja, M.A.Z.; Shoaib, M.; Tabassum, R.; Khan, N.M.; Kehili, S.; Bafakeeh, O.T. Stochastic numerical computing for entropy optimized of Darcy-Forchheimer nanofluid flow: Levenberg Marquardt Algorithm. *Chem. Phys. Lett.* **2022**, *807*, 140070. [[CrossRef](#)]
39. Shoaib, M.; Tabassum, R.; Nisar, K.S.; Raja, M.A.Z.; Fatima, N.; Al-Harbi, N.; Abdel-Aty, A.H. A design of neuro-computational approach for double-diffusive natural convection nanofluid flow. *Heliyon* **2022**, *9*, e14303. [[CrossRef](#)] [[PubMed](#)]
40. Shoaib, M.; Zubair, G.; Nisar, K.S.; Raja, M.A.Z.; Khan, M.I.; Gowda, R.P.; Prasannakumara, B.C. Ohmic heating effects and entropy generation for nanofluidic system of Ree-Eyring fluid: Intelligent computing paradigm. *Int. Commun. Heat Mass Transf.* **2021**, *129*, 105683. [[CrossRef](#)]
41. Ali, I.; Gul, T.; Khan, A. Unsteady Hydromagnetic Flow over an Inclined Rotating Disk through Neural Networking Approach. *Mathematics* **2023**, *11*, 1893. [[CrossRef](#)]

Disclaimer/Publisher’s Note: The statements, opinions and data contained in all publications are solely those of the individual author(s) and contributor(s) and not of MDPI and/or the editor(s). MDPI and/or the editor(s) disclaim responsibility for any injury to people or property resulting from any ideas, methods, instructions or products referred to in the content.